

Augmented Reality without Borders: Achieving Precise Localization Without Maps

Albert Gassol Puigjaner, Irvin Aloise and Patrik Schmuck

Abstract—Visual localization is crucial for Computer Vision and Augmented Reality (AR) applications, where determining the camera or device’s position and orientation is essential to accurately interact with the physical environment. Traditional methods rely on detailed 3D maps constructed using Structure from Motion (SfM) or Simultaneous Localization and Mapping (SLAM), which is computationally expensive and impractical for dynamic or large-scale environments. We introduce MARLOC, a novel localization framework for AR applications that uses known relative transformations within image sequences to perform intra-sequence triangulation, generating 3D-2D correspondences for pose estimation and refinement. MARLOC eliminates the need for pre-built SfM maps, providing accurate and efficient localization suitable for dynamic outdoor environments. Evaluation with benchmark datasets and real-world experiments demonstrates MARLOC’s state-of-the-art performance and robustness. By integrating MARLOC into an AR device, we highlight its capability to achieve precise localization in real-world outdoor scenarios, showcasing its practical effectiveness and potential to enhance visual localization in AR applications.

I. INTRODUCTION

Augmented Reality (AR) is a relatively new technology, and the research community is investigating ways to leverage this technology in several fields, ranging from medical applications over navigation to video games. One of the main characteristics that makes AR so appealing is its ability to seamlessly blend digital content with the real world. This allows users to interact simultaneously with the physical environment and its digitally enhanced counterpart. Consequently, the ability to accurately distribute *world-locked* virtual content in physical environments is extremely valuable for successfully creating AR applications.

In this context, the well-established topic of Visual Localization is a fundamental building block for creating such world-locked immersive and interactive AR experiences, since it allows to exactly determine the position of the AR device within the environment. With Visual Localization, we refer to the Computer Vision problem of determining the position and orientation of an image with respect to another image. Traditional methods solve this problem by relying on a digital reconstruction of the geometry of the environment, typically resorting to techniques such as SfM [1] or SLAM [2], [3], [4] to construct pointclouds used at localization time [5], [6], [7]. This family of approaches has been proven to be very effective, however, they also come with several

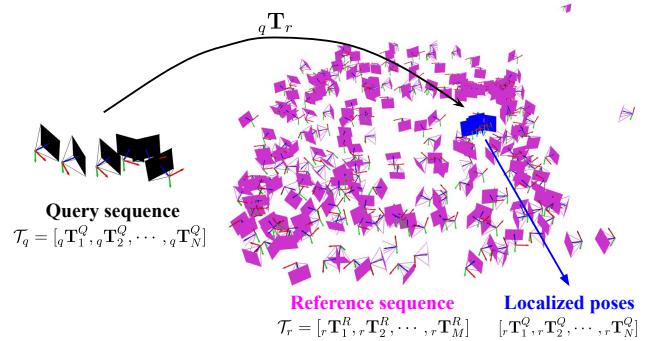


Fig. 1: Given a sequence of **locally posed query frames** \mathcal{T}_q and a set of **posed reference frames** \mathcal{T}_r , our objective is to find $\{{}_r\mathbf{T}_1^Q, {}_r\mathbf{T}_2^Q, \dots, {}_r\mathbf{T}_N^Q\}$, i.e. the **localized query frames** poses with respect to the reference frame. Our approach does not need any prior geometry relative to the reference images (e.g. triangulated feature points), but it only relies on posed reference images to achieve this task.

shortcomings. As the main drawback, creating a digital representation of the geometry of the environment (commonly referred to as a *map*) is a computationally demanding and time-consuming operation. To have some grounding, an SfM-based reconstruction of an office-like environment can take hours to complete on a powerful workstation [8], which can constitute a problem for interactive AR applications where compute resources are rather limited and impose a long wait for the user to interact with the AR experience. Furthermore, the images employed in the processing are required to have a good overlap for the reconstruction to be successful. Faster ways of creating maps from a sequence of images exist in the literature; however, approaches like SLAM usually require additional sensor inputs - e.g. Inertial Measurement Unit (IMU) [9], [10], [11] - to succeed and often result in very sparse maps, which are not optimal for visual localization algorithms. Finally, oftentimes it is not practical to manually capture images for the reference environment, making it complex to perform any sort of prior reconstruction, such as when operating in large outdoor environments or deploying AR experiences in distant places. Given this, the research community is investigating ways of generating accurate visual localization estimates in *map-free* setups [12], only using a sparse set of images as a digital representation of the reference environment. This setup allows us to avoid performing expensive mapping sessions to prepare the localization framework and streamlines the overall integration in real-time applications such as AR.

In this letter, we introduce MARLOC (Map-free Augmented Reality Localization), a novel visual localization framework for AR applications. Our approach uses a se-

quence of query images to create a local representation of the 3D structure around the current position of the user and then leverages this local representation to accurately estimate the relative pose to a given world-registered reference image. We extensively evaluate MARLOC against several established methods for both map-free and map-based visual localization, demonstrating its state-of-the-art (SOTA) performance in robustness and accuracy among map-free approaches.

While most of the existing literature shows functionality only on pre-recorded benchmark datasets, leaving the practicality of the approach open, we additionally demonstrate the real-world applicability of MARLOC in a real-world scenario with a Magic Leap 2¹ AR headset and Mapillary² reference images. To the best of our knowledge, this is the first real-world demonstration of a map-free localization approach with a commercially available AR headset.

In summary, our key contributions are threefold:

- We introduce MARLOC, a novel method for *map-free localization*.
- We extensively evaluate MARLOC on benchmark datasets, attesting to its competitive performance compared to the current SOTA in map-free localization.
- We conduct a real-world experiment, demonstrating the practical applicability of MARLOC with a commercially available AR headset.

II. RELATED WORKS

Visual Localization is an established problem in the Computer Vision and Robotics community. Although several methods have been introduced over the years to efficiently solve this problem using the existing geometry of the reference environment [13], our paper focuses on map-free scenarios [12], which are particularly relevant for AR applications.

Structure-Based Localization. Traditional structure-based visual localization methods [5], [6], [7], [13] estimate camera poses by first building a 3D map via SfM [1], and then finding correspondences between the map features and local image descriptors [14], [15], [16], [17], [18], [19], [20], [21], [22]. Large-scale localization approaches tackle this problem in a hierarchical fashion, leveraging image retrieval [23], [24], [25], [26], [27] to reduce the search space of feature matching, keeping the computational complexity of the solution relatively bounded. These methods are the typical choice of visual localization when a large number of images are available to construct a map. However, sparsity in the number of images can lead to a lack of viewpoint overlap, thus highly decreasing the quality of the map’s structure. Additionally, building a map requires an explicit mapping session, which can, including post-processing, take multiple hours for medium-sized environments. This may impose a significant burden or not be possible at all, depending on the application. On the contrary, our method does not require the user to perform an explicit mapping session to achieve accurate localization results.

¹<https://www.magicleap.com/magic-leap-2>

²<https://www.mapillary.com>

Keypoint Matching + Depth Estimation. Given two images with enough overlap and known intrinsics, the relative transformation between them can be estimated through essential matrix decomposition [28], [29], [30] by making use of local 2D features. Still, this family of methods can only estimate the relative translation vector up to an unknown scale. If additional depth information is available, the problem can be solved using Perspective-n-Point (PnP) algorithms [31] or 3D-3D registration techniques [32], [33]. Recent advancements in deep learning resulted in several frameworks to estimate depth from a monocular image [34], [35], [36], [37], and the community has investigated their usage for map-free localization purposes [12]. However, the accuracy of the localization outcome is bounded by the accuracy of the depth estimation methods, which might struggle to have consistent depth predictions around corners and edges - *i.e.* typical parts of the images where 2D features are extracted. While these methods rely on monocular depth estimation to lift keypoints into 3D space, our method overcomes this limitation by leveraging known relative transformations between the query sequence of images to infer the 3D geometry of keypoints.

Relative Pose Regression (RPR) . Recent deep learning approaches directly estimate the relative transformation between two images [38], [39], [40], [41], [12]. These methods use a single network to extract encodings of both images and use them to regress an estimate of the relative transformation between the images. However, these methods cannot predict the quality confidence of the regressed pose, which is often useful to discard estimates when there is not enough overlap between the images, ultimately resulting in many outliers in the estimated poses. Additionally, these methods are often less accurate than matching-based approaches when image overlap is not a limiting factor.

Differential RANSAC. RANSAC [42] is a robust method to estimate the parameters of a mathematical model. Differentiating RANSAC [43], [44] allows one to learn the relative pose between two images in an end-to-end manner. MicKey [45] proposes to leverage differential RANSAC to directly learn the 3D-3D correspondences between two images end-to-end. Similarly to [46], MicKey uses the relative pose between the two images as the only supervision signal. While this family of method gains some robustness over RPR from leveraging RANSAC, accuracy is still limited compared to structure-based approaches.

Image matching in 3D. Wang *et al.* propose DUST3R [37], leveraging Vision Transformers [47] (ViTs) to regress a dense scene representation from a pair of images in an end-to-end manner. The scene representation encapsulates a pointcloud together with its 2D-3D correspondences with the pair of images. The recently introduced MAST3R [48] builds upon DUST3R to add a new head that outputs dense local features, which is trained with a matching loss. This approach significantly improves the absolute pose estimation capabilities of DUST3R and achieves SOTA results in map-free localization. However, these methods still lack the precision achieved by structure-based approaches.

III. PROBLEM STATEMENT

Notation. In the remainder of this document, ${}_i\mathbf{T}_j \in \text{SE}(3)$ denotes the 6-Degrees of Freedom (DoF) transformation from coordinate frame j to frame i . ${}_i\mathbf{T}_j = [{}_i\mathbf{R}_j | {}_i\mathbf{t}_j]$ is parametrized by a rotation ${}_i\mathbf{R}_j \in \text{SO}(3)$ and a translation ${}_i\mathbf{t}_j \in \mathbb{R}^3$. We denote q and r as the query and reference frames, respectively. $\mathbf{p}_{i,k}^q$ denotes the image coordinate of the k -th 2D keypoint of image I_i^q corresponding to the query sequence; similarly, $\mathbf{p}_{j,k}^r$ denotes a keypoint of the reference image I_j^r . $\mathbf{P}_{i,k}^q$ denotes the triangulated 3D pose in the query frame of the k -th keypoint of image I_i^q corresponding to the query sequence.

Objective. Given a sequence of N posed query images $\mathcal{I}_q = \{I_1^q \cdots I_N^q\}$ with corresponding poses $\mathcal{T}_q = \{{}_q\mathbf{T}_1^Q \cdots {}_q\mathbf{T}_N^Q\}$ in the query frame q , and a set of M posed reference images $\mathcal{I}_r = \{I_1^r \cdots I_M^r\}$ with corresponding poses $\mathcal{T}_r = \{{}_r\mathbf{T}_1^R \cdots {}_r\mathbf{T}_M^R\}$ in the reference frame r , our goal is to find the query frame poses with respect to the reference frame - *i.e.* $\{{}_r\mathbf{T}_1^Q \cdots {}_r\mathbf{T}_N^Q\}$. Note that, in the extent of this paper, we assume to have no prior geometry associated with the reference images, meaning that, no explicit mapping stage via SLAM or SfM has to be performed by the user - reference images and associated poses in the reference frame are sufficient to use MARLOC. We present a visual representation of the problem statement in Fig. 1.

IV. METHOD

We introduce MARLOC, a novel pipeline for map-free localization. Our approach takes as input a sequence of monocular images or rigs with multiple images posed in the query reference frame, together with one or more reference images located in a different (global) reference frame. The output is the set of 6DoF poses relative to each individual query image expressed in the global reference frame. Note that no prior geometry is required for MARLOC to work. Since AR devices are required to track their motion through the environment to display world-registered content, the relative poses of the query frames can be easily obtained from the onboard Visual-Inertial Odometry (VIO) or SLAM system of the AR device, such as *ARKit*, *ARCore*, or *Magic Leap's Head Tracking*. Therefore, we assume that these poses are given, and estimating them is outside the scope of this method.

In the remainder of this section, we outline the main individual components of our approach, summarized in Fig. 2. We start by performing feature extraction and candidate selection in Sec. IV-A, which is followed by local feature extraction and matching. We then lift the query 2D features by performing intra-sequence triangulation in Sec. IV-B. Finally, we make use of the triangulated points to perform pose estimation and refine our pose estimates through relative pose graph optimization in Sec. IV-C.

A. Candidate Selection and Matching

Following LaMAR [13], we extract a fusion [49] of the NetVLAD [23] and APGeM [24] descriptors for all query

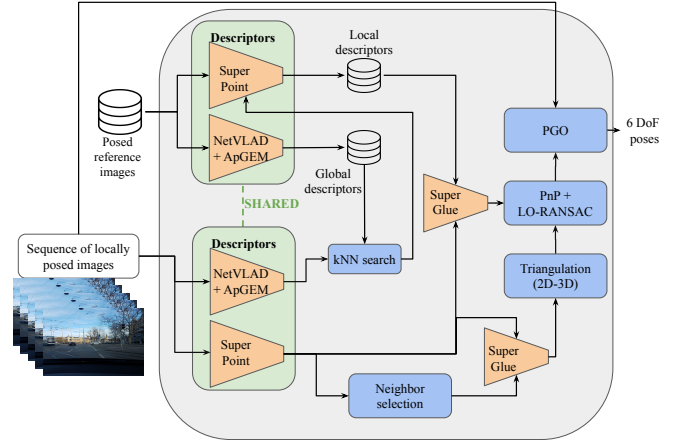


Fig. 2: The query frames are localized using only reference images from the database. MARLOC uses NetVLAD [23] + APGeM [24] for image retrieval, while SuperPoint [17] and SuperGlue [21] are used to extract and match local descriptors. We triangulate query 3D points by leveraging the prior poses of the query frames, allowing us to perform pose estimation via the PnP algorithm. The final set of query poses is refined via Pose-Graph Optimization (PGO).

and reference images. We make use of the extracted descriptors to perform image retrieval on the reference images. Thus, for each query image I_i^q we select the closest reference images $K \{I_j^r\}_{1 \leq j \leq K}$, referred to as *candidates*.

Subsequently, we use SuperPoint [17] to extract local features from the query sequence and the selected candidate images from the reference set. Then, we use SuperGlue [21] to perform feature matching and obtain a set of 2D-2D correspondences. Formally, for each query image I_i^q and its selected candidate reference images $\{I_j^r\}_{1 \leq j \leq K}$, we obtain the 2D-2D correspondences $\{\mathbf{p}_{i,k}^q \mathbf{p}_{j,k}^r\}_k$.

B. Intra-sequence Query Keypoints Triangulation

Common visual localization algorithms extract 2D-3D correspondences by lifting the keypoints of reference images, either using previously built geometry representations of the reference environment [13], [7], [5], [1] - *e.g.* sparse or dense point clouds - or leveraging depth information from additional sensors or extracted from the monocular image [12]. In this work, we propose to make use of the known relative transformations between frames of the query sequence to triangulate 2D keypoints and lift them to 3D. These 3D points are used to construct 3D-2D correspondences between the query and reference frames. In the remainder, we describe the proposed steps to triangulate query keypoints.

Neighbor selection. To perform intra-sequence triangulation on the query images, we first select a neighbor image (from within the query sequence) for each query image. Since we need a minimum of parallax between a query frame and its selected neighbor, we propose to use Alg. 1, which performs a simple distance check on the rotational and translational displacement between the two. Thus, for query image I_i^q , we select its neighbor as the first frame in the sequence whose relative pose compared to the query frame is larger than a user-specified threshold $(\mathbf{t}_{min}, \theta_{min})$. For each query frame, if a neighbor is not found due to a lack of distance between query frames, the pose estimation for the respective query

frame is skipped.

Algorithm 1 Neighbor Selection

```

1: Input:  $\mathcal{T}_q, \mathbf{t}_{min}, \theta_{min}$ 
2:  $\mathcal{N}_q \leftarrow \emptyset$ 
3: for  $i = 0, \dots, N - 1$  do
4:   for  $j = i + 1, \dots, N$  do
5:      ${}_i\mathbf{T}_j^e \leftarrow ({}_q\mathbf{T}_i)^{-1} {}_q\mathbf{T}_j$ 
6:      ${}_i\mathbf{q}_j^e \leftarrow \text{rot2quat}({}_j\mathbf{R}_i^e)$ 
7:      $\theta^e \leftarrow \text{atan2}(\|{}_i\mathbf{q}_j^e[x, y, z]\|_2, \|{}_i\mathbf{q}_j^e[w]\|_1)$ 
8:     if  $\|{}_i\mathbf{t}_j\|_2 \geq \mathbf{t}_{min}$  and  $\theta^e \geq \theta_{min}$  then
9:        $\mathcal{N}_q[i] \leftarrow j$ 
10:    break
11:   end if
12: end for
13: end for
14: return  $\mathcal{N}_q$ 

```

Feature matching and triangulation. Next, we match local features for each query sequence image and their corresponding neighbor. Thus, for each query image I_i^q and its corresponding neighbor, denoted as $\mathcal{N}_q[i]$, we obtain a set of 2D-2D correspondences $\{\mathbf{p}_{\mathcal{N}_q[i],k}^q, \mathbf{p}_{i,k}^q\}_k$. Consecutively, we make use of the matches to triangulate 3D points in the query frame using their poses ${}_q\mathbf{T}_i^Q$ and ${}_q\mathbf{T}_{\mathcal{N}_q[i]}^Q$, obtaining $\{\mathbf{p}_{i,k}^q, \mathbf{p}_{i,k}^q\}_k$.

3D-2D correspondences. Finally, we extract 3D-2D correspondences between the reference and query frames by selecting the 2D keypoints present in both the query to reference images 2D-2D matches $\{\mathbf{p}_{i,k}^q, \mathbf{p}_{j,k}^r\}_k$ and the query to neighbor 2D-2D matches $\{\mathbf{p}_{\mathcal{N}_q[i],k}^q, \mathbf{p}_{i,k}^q\}_k$. Thus, for each query and retrieved reference images, we obtain a set of 3D-2D correspondences: $\mathcal{M}_i = \bigcup_{j=1}^K \{\mathbf{p}_{i,k}^q, \mathbf{p}_{j,k}^r\}_k$.

C. Pose Estimation and Pose Graph Optimization (PGO)

Having computed the 3D-2D correspondences \mathcal{M}_i , we employ a standard PnP [31] algorithm to obtain an initial estimate of the query poses with respect to the reference frame, namely ${}_r\mathbf{T}_i^{Q,init}$. To this end, we employ the pose estimation module available in COLMAP [1], which makes use of a LO-RANSAC [50] stage and a non-linear refinement. Note that we discard all poses that contain a number of inliers lower than a user-specified threshold. This can happen due to a lack of texture, not enough overlap, difficult lighting conditions, or domain changes - e.g. weather and seasons.

As a final step, we refine our pose estimates by leveraging relative Pose Graph Optimization (PGO) [51] between the estimated poses and the localization queries. In detail, we compute the optimal set of poses ${}_r\mathbf{T}_i^{Q,PGO}$ that minimize the following cost function:

$$\min_{{}_r\mathbf{T}_i^{Q,PGO}} \sum_{i=1}^{N-1} \mathbf{e}_i^T \Sigma^{-1} \mathbf{e}_i,$$

where each cost factor i is an SE(3) constraint defined as

$$\mathbf{e}_i = \left(({}_r\mathbf{T}_{i+1}^{Q,PGO})^{-1} {}_r\mathbf{T}_i^{Q,PGO} \right) \boxminus \left(({}_q\mathbf{T}_{i+1}^Q)^{-1} {}_q\mathbf{T}_i^Q \right), \quad (1)$$

and $\Sigma \in \mathbb{R}^{6 \times 6}$ is the covariance matrix of the localization queries provided by the on-device VIO or SLAM system. The \boxminus operator defined in Eq. (1) is a non-linear mapping $\text{SE}(3) \rightarrow \mathbb{R}^n$ that computes the local distance between the two poses in the manifold [52], [53]. Furthermore, we employ a robust loss function to handle eventual outliers in the optimization [54], [55], [56].

With this operation, we use the information stored in the query poses, computed by the on-device SLAM or VIO system, to constrain the relative motion of subsequent localization estimates. We initialize the optimizable poses ${}_r\mathbf{T}_i^{Q,PGO}$ to ${}_r\mathbf{T}_i^{Q,init}$, which have been estimated previously with PnP and LO-RANSAC. Additionally, to avoid an ill-posed formulation, we fix the pose ${}_r\mathbf{T}_i^{Q,PGO}$ with the most number of inliers.

V. EXPERIMENTS

In this section, we provide quantitative and qualitative results obtained with our MARLOC pipeline. We compare MARLOC with the most recent SOTA methods in the field for map-free localization, and demonstrate our proposed approach in a real-world AR setting, using a Magic Leap ML2 device and the Mapillary crowd-sourced database to precisely register digital content with the physical world. To the best of our knowledge, this is the first time that a map-free visual-localization pipeline has been integrated into a commercially available AR headset.

Implementation Details. We integrate our proposed method into the localization framework provided by LaMAR [13]³. To select a neighbor for each query frame, we set the minimum distance thresholds used in Alg. 1 to $\mathbf{t}_{min} = 0.3m$ and $\theta_{min} = 10^\circ$. The default configurations [13] for NetVLAD [23], ApGEM [24], SuperPoint [17] and SuperGlue [21] are used. When triangulating 3D points from 2D-2D correspondences between a query and its neighbor, we allow for a maximum reprojection error of 3 pixels. Additionally, we apply the same maximum reprojection error during pose estimation (Sec. IV-C). Finally, we set the sequence query batch $N = 10$. The queries in a sequence are consecutive (i.e. timestamp ordered) in all datasets and when testing with the AR device. Each batch is processed individually and does not incorporate localization results from previous batches into the process.

Datasets. MARLOC is evaluated in two datasets: the Niantic Map-Free Relocalization Dataset [12] and the LaMAR dataset [13]. The Niantic Map-Free Relocalization Dataset is the standard benchmark of map-free localization methods. It consists of 655 outdoor scenes containing small places of interest. The dataset is split into 460 training scenes, 65 validation scenes, and 130 test scenes. Each scene contains a single reference image and a set of approximately 500 query images. In this work, we use the validation dataset only to generate localization queries, since the ground truth poses of the query images with respect to the reference image are provided. The LaMAR dataset is a large-scale

³<https://github.com/microsoft/lamar-benchmark>

dataset captured using AR devices, and, hence, the results provide insights into how well each method performs in real-world AR settings. Specifically, three different sessions (CAB, HBE and LIN) are captured, containing both indoor and outdoor environments. Each session includes a mapping sequence, which we use as a reference, and two validation query sequences (captured with a Microsoft HoloLens 2⁴ and hand-held Apple iPhone/iPad) which include ground truth poses with respect to the mapping sequence.

Baselines. We compare MARLOC against SOTA methods in map-free localization: **i)** MicKey [45], **ii)** Relative Pose Regression parametrized with a 6D parametrization for the rotation (referred to as RPR $[R(6D) + t]$ [12], [57], **iii)** feature matching (with SuperPoint and SuperGlue) with essential matrix estimation and scale from monocular depth from [12] (shortened as E+D), and **iv)** MAST3R [48]. Furthermore, we include comparisons with the LaMAR [13] framework, as representative of structure-based hierarchical localization. The comparison with the LaMAR pipeline has been performed using the companion dataset from the same authors, providing insights of how well the proposed approach performs compared to the current gold standard in visual localization.

Metrics. Following [13], [12], we evaluate MARLOC and the baselines using the median Absolute Pose Error (APE), both in translation and rotation. Additionally, we evaluate the recall at different translation and rotation error thresholds. Furthermore, we report the time required to localize a query image sequence.

A. Niantic Map-Free Relocalization Dataset

In our comparisons, we include all map-free baselines. Note that in this dataset, the number of candidates used in our method K is always 1, since there is only one reference image per scene. Therefore, LaMAR is not evaluated in this dataset since structure cannot be extracted from a single reference image. Tab. I presents the main results on the Niantic Map-Free dataset. As shown, our method achieves SOTA results in terms of median APE. The table additionally shows the percentage of localized queries. Methods that use matching - *i.e.* ours and E+D - take into account the number of inliers to reject outlier queries when this number is low. For this reason, the percentage of localized queries in MicKey and RPR $[R(6D) + t]$ is higher compared to the matching-based methods, however, at the cost of significantly reduced average accuracy.

Fig. 3 presents the APE values evaluated on each scene of the dataset. Our method concentrates most of the samples at low values, while other baselines present a larger spread, which attests to the robust performance of our MARLOC. We additionally showcase the recall at different APE thresholds in Fig. 4. As visible from the figures, MARLOC achieves a higher recall than all baselines at any APE.

⁴<https://www.microsoft.com/en-us/hololens>

⁵Results for MAST3R on the Niantic Map-Free dataset as reported in [48].

	Median APE	Average query time	% localized queries
MicKey [45]	94.7 cm, 14.52°	19.68 s	100
RPR $[R(6D) + t]$ [12]	123 cm, 15.31°	0.04 s	100
E+D [12]	57.5 cm, 2.28°	0.03 s	51.76
MASt3R [48] ⁵	35 cm, 2.2°	N/A	N/A
MARLOC (ours)	5.55 cm, 0.80°	0.33 s	59.27

TABLE I: We present a comparison of the median APE achieved by our method and the baselines using the **Niantic Map-Free dataset**. We additionally present the time per query achieved by each method and the percentage of localized queries. Our method clearly outperforms the baselines in terms of APE. **Best result.** **Second best result.**

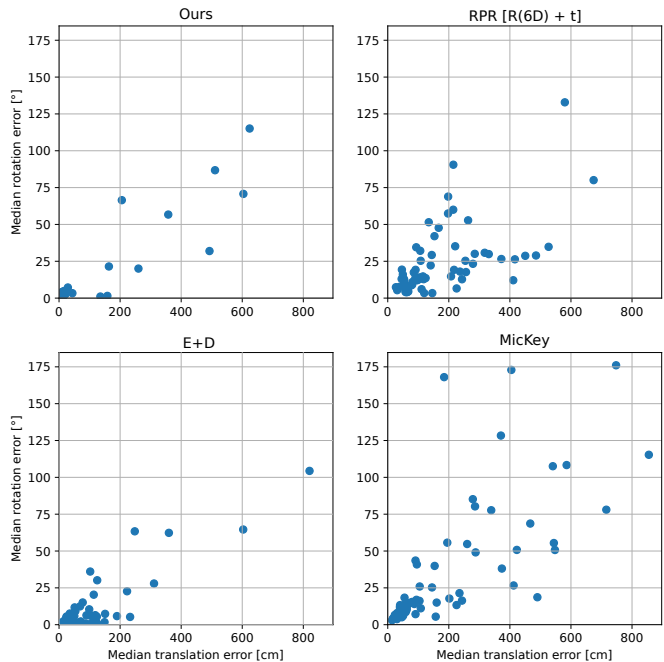


Fig. 3: Median rotation error against median translation error for each scene of the **Niantic Map-Free dataset**. The error distribution of our approach is concentrated in the bottom-left corner, with the center of mass in a low-error range.

B. LaMAR Dataset

MARLOC is compared against MicKey and LaMAR in the LaMAR dataset. We do not evaluate RPR $[R(6D) + t]$ and E+D on this dataset, since retraining is required for both the regression and monocular depth estimation models. To have a fair evaluation, we present the results of LaMAR and our method using $K = 1$ and $K = 10$ retrieved reference image candidates since MicKey cannot use more than one retrieved candidate for pose estimation. We present quantitative results in Tab. II. Our method produces significantly more accurate localization estimates compared to the other map-free pipelines evaluated on this dataset. Furthermore, the metrics obtained are in a similar range with the well-established LaMAR pipeline, without the need for an explicit SfM-based mapping session. Note that LaMAR and MARLOC are more conservative when localizing a query compared to MicKey, since we restrict the minimum number of inliers during pose estimation. This is reflected in a lower percentage of localized queries for both LaMAR and MARLOC, but also in significantly higher accuracy.

	Median APE			Avg. Query Time			% Localized		
	CAB	HGE	LIN	CAB	HGE	LIN	CAB	HGE	LIN
MicKey [45]	427 cm, 25.29°	459 cm, 19.75°	255 cm, 17.62°	3.43 s	3.96 s	13.92 s	93.88	95.08	96.09
LaMAR ($K = 10$) [13]	3.25 cm, 0.30°	4.64 cm, 0.26°	1.96 cm, 0.17°	2.89 s	5.83 s	9.15 s	83.81	86.45	85.35
LaMAR ($K = 1$) [13]	3.58 cm, 0.34°	6.29 cm, 0.30°	2.17 cm, 0.18°	0.52 s	0.86 s	1.28 s	54.11	66.89	72.65
MARLOC ($K = 10$) (Ours)	7.44 cm, 0.52°	14.06 cm, 0.45°	5.44 cm, 0.27°	1.96 s	1.98 s	1.60s	66.83	93.91	88.98
MARLOC ($K = 1$) (Ours)	8.86 cm, 0.57°	18.1 cm, 0.50°	6.51 cm, 0.37°	0.21 s	0.29 s	0.27 s	57.15	86.32	80.56

TABLE II: We present a comparison of the median APE achieved by our method and the baselines using the **LaMAR dataset**. We additionally present the time per query achieved by each method and the percentage of localized queries. Our pipeline achieves significantly better results compared to MicKey, producing metrics in the same range as LaMAR without the need for an explicit SfM session. **Best result. Second best result.**

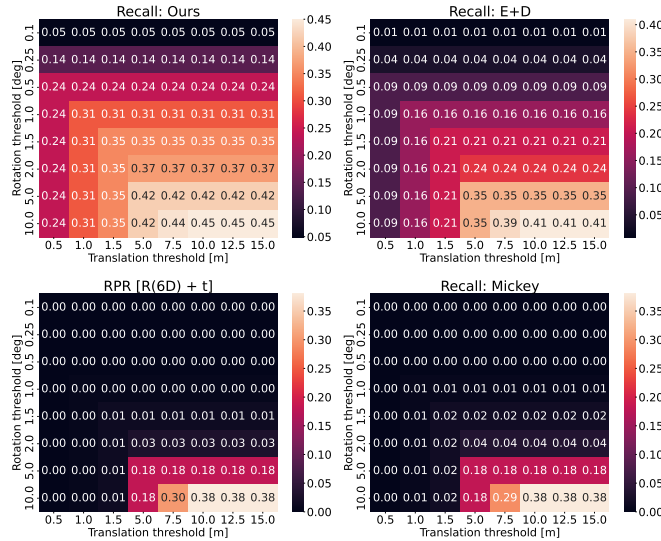


Fig. 4: Recall in **Niantic Map-Free dataset** at different APE thresholds. Best viewed when zoomed in.

Furthermore, we report in Fig. 5 the recall of the three methods, evaluated at different pose error thresholds. MARLOC significantly outperforms the other map-free methods and exhibits metrics in a similar range to the LaMAR framework, despite not using any prior structure at localization time.

C. AR Device Testing

Setup. To demonstrate the practicality of our approach in AR applications, we use MARLOC together with a Magic Leap 2 (ML2) device in a live, real-world experiment. The ML2 is equipped with a sensor rig that includes three cameras, specifically designed to accommodate Computer Vision algorithms, and has its own proprietary perception stack onboard. We collect ML2 *rig-frames* (a frame combining one image per camera) at sensor rate as query images, while pose estimates for each frame are provided by the native SLAM system of the ML2 and therefore expressed in the device reference frame q . Each *localization query* is composed of a set of $N = 10$ posed rig-frames.

The images used as a reference for localization are taken from the public Mapillary database. Mapillary provides geolocation information about each image - *i.e.* latitude, longitude and altitude - and it also exposes intrinsic parameters of the camera setup. These Mapillary images and their geolocation are used as the reference sequence \mathcal{I}_r . Our goal

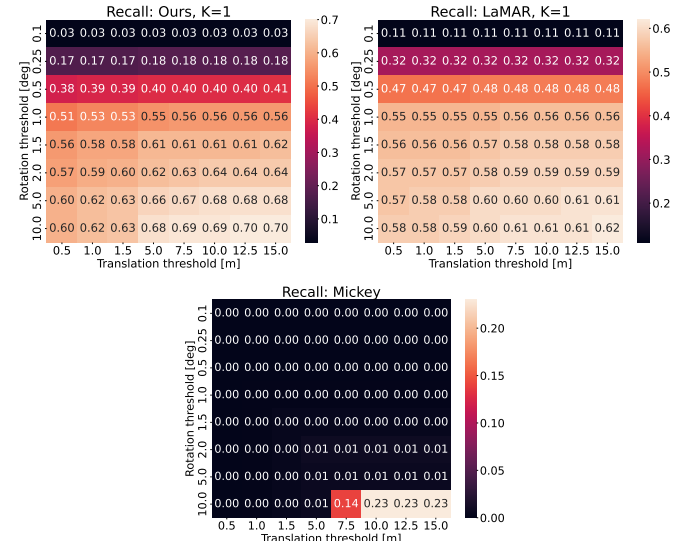


Fig. 5: Recall in **LaMAR benchmark** at different APE thresholds. Best viewed when zoomed in.

is to capture sequences of images with an ML2 and use them to localize the AR device with respect to a global frame of reference using Mapillary imagery.

Qualitative evaluation. In the absence of accurate ground-truth data in this setup, we evaluate the performance of our method with the ML2 device using the following procedure: (i) First, we employ our method to localize the ML2 within the global frame of reference. (ii) Next, we place example visual content (in our experiments a virtual 3D coordinate frame) at various distinguishable physical locations within this global frame based on the initial localization event. (iii) Finally, we use our method to relocalize the ML2 with respect to the global frame from a different point of view. Accurate localization is indicated if the visual content remains close to its initial position. Fig. 6 showcases a qualitative evaluation of our method using the described setup. As presented, the visual content (3D coordinate system) remains in a similar position throughout the three localization events. The colored bounding boxes highlight the same selected virtual content after successive localization events throughout the experiment. In addition to Fig. 6, the video ⁶ accompanying this article shows the experiment described in this section.

⁶<https://youtu.be/t47D-4-F1FI>

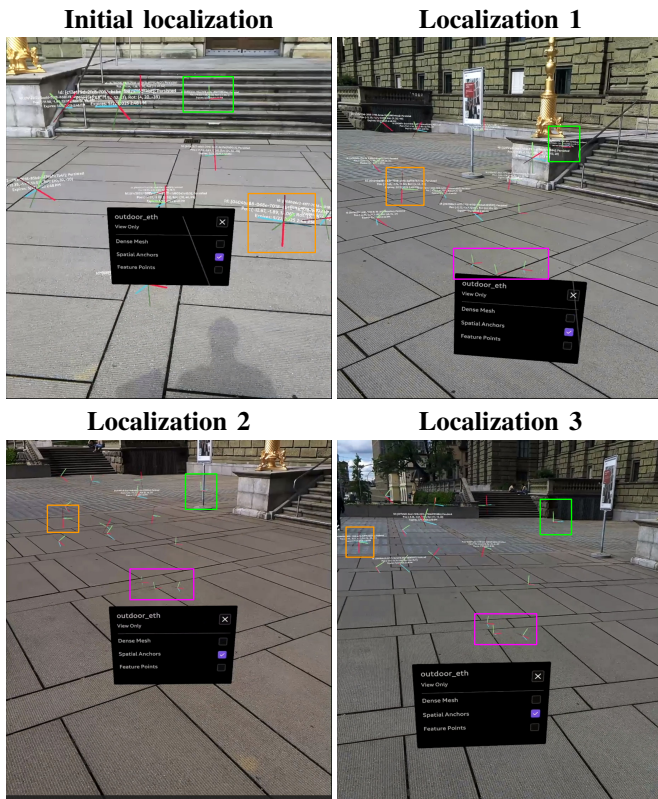


Fig. 6: Visual content after several localization events using our method integrated into an ML2 device. The visual content is placed after the initial localization. After each localization event, the visual content remains close to its original position in the physical space. The bounding boxes distinguish different visual content at each localization event.

VI. CONCLUSIONS

In this letter we introduce a novel map-free visual localization framework for AR applications - namely MARLOC. Our approach leverages the known relative transformations of the query sequence to perform intra-sequence triangulation and lift 2D-2D matches into the 3D space, followed by pose estimation with PnP and further refinement with PGO. Our evaluation on benchmark datasets for map-free and map-based localization showcases the competitive performance of MARLOC compared to other SOTA methods addressing the map-free case. Furthermore, MARLOC achieves results within the same range as traditional SfM-based localization approaches, which are the gold standard in visual localization, but without requiring the use of a time- and compute-intensive mapping phase. Finally, we test our method in a real-world experiment using a Magic Leap 2 AR device and publicly available map data from Mapillary, attesting to the practicality of MARLOC for AR use-cases.

REFERENCES

- [1] J. L. Schönberger and J.-M. Frahm, “Structure-from-motion revisited,” *CVPR*, 2016.
- [2] S. Thrun, W. Burgard, and D. Fox, *Probabilistic robotics*. MIT Press, 2005.
- [3] G. Grisetti, R. Kümmerle, C. Stachniss, and W. Burgard, “A tutorial on graph-based slam,” *IEEE Trans. Intell. Transport. Syst.*, 2010.
- [4] R. Mur-Artal, J. M. M. Montiel, and J. D. Tardós, “ORB-SLAM: a versatile and accurate monocular SLAM system,” *T-RO*, 2015.

- [5] J. L. Schönberger, E. Zheng, M. Pollefeys, and J.-M. Frahm, “Pixel-wise view selection for unstructured multi-view stereo,” *ECCV*, 2016.
- [6] T. Sattler, B. Leibe, and L. Kobbelt, “Improving image-based localization by active correspondence search,” *ECCV*, 2012.
- [7] P.-E. Sarlin, C. Cadena, R. Siegwart, and M. Dymczyk, “From coarse to fine: Robust hierarchical localization at large scale,” *CVPR*, 2019.
- [8] E. Brachmann, T. Cavallari, and V. A. Prisacariu, “Accelerated coordinate encoding: Learning to relocalize in minutes using rgb and poses,” *CVPR*, 2023.
- [9] J. Delmerico and D. Scaramuzza, “A benchmark comparison of monocular visual-inertial odometry algorithms for flying robots,” *ICRA*, 2018.
- [10] M. Bloesch, S. Omari, M. Hutter, and R. Siegwart, “Robust visual inertial odometry using a direct ekf-based approach,” *IROS*, 2015.
- [11] C. Forster, L. Carlone, F. Dellaert, and D. Scaramuzza, “On-manifold preintegration for real-time visual-inertial odometry,” *T-RO*, 2015.
- [12] E. Arnold, J. Wynn, S. Vicente, G. Garcia-Hernando, Á. Monszpart, V. A. Prisacariu, D. Turmukhambetov, and E. Brachmann, “Map-free visual relocalization: Metric pose relative to a single image,” *ECCV*, 2022.
- [13] P.-E. Sarlin, M. Dusmanu, J. L. Schönberger, P. Speciale, L. Gruber, V. Larsson, O. Miksik, and M. Pollefeys, “Lamar: Benchmarking localization and mapping for augmented reality,” *ECCV*, 2022.
- [14] D. G. Lowe, “Distinctive image features from scale-invariant keypoints,” *IJCV*, 2004.
- [15] H. Bay, T. Tuytelaars, and L. Van Gool, “Surf: Speeded up robust features,” *ECCV*, 2006.
- [16] E. Rublee, V. Rabaud, K. Konolige, and G. R. Bradski, “Orb: An efficient alternative to sift or surf,” *ICCV*, 2011.
- [17] D. DeTone, T. Malisiewicz, and A. Rabinovich, “Superpoint: Self-supervised interest point detection and description,” *CVPR*, 2018.
- [18] M. Dusmanu, I. Rocco, T. Pajdla, M. Pollefeys, J. Sivic, A. Torii, and T. Sattler, “D2-net: A trainable cnn for joint description and detection of local features,” *CVPR*, 2019.
- [19] J. Revaud, P. Weinzaepfel, C. R. de Souza, and M. Humenberger, “R2D2: repeatable and reliable detector and descriptor,” *NIPS*, 2019.
- [20] K. M. Yi, E. Trulls, V. Lepetit, and P. V. Fua, “Lift: Learned invariant feature transform,” *ECCV*, 2016.
- [21] P.-E. Sarlin, D. DeTone, T. Malisiewicz, and A. Rabinovich, “Super-Glue: Learning feature matching with graph neural networks,” *CVPR*, 2020.
- [22] P. Lindenberger, P.-E. Sarlin, and M. Pollefeys, “LightGlue: Local Feature Matching at Light Speed,” *ICCV*, 2023.
- [23] R. Arandjelović, P. Gronát, A. Torii, T. Pajdla, and J. Sivic, “Netvlad: Cnn architecture for weakly supervised place recognition,” *CVPR*, 2015.
- [24] J. Revaud, J. Almazan, R. S. Rezende, and C. R. d. Souza, “Learning with average precision: Training image retrieval with a listwise loss,” *ICCV*, 2019.
- [25] B. Cao, A. F. de Araújo, and J. Sim, “Unifying deep local and global features for image search,” *ECCV*, 2020.
- [26] A. Rau, G. Garcia-Hernando, D. Stoyanov, G. J. Brostow, and D. Turmukhambetov, “Predicting visual overlap of images through interpretable non-metric box embeddings,” *ECCV*, 2020.
- [27] G. Tolas, Y. Avrithis, and H. Jégou, “To aggregate or not to aggregate: Selective match kernels for image search,” *ICCV*, 2013.
- [28] R. I. Hartley and A. Zisserman, *Multiple View Geometry in Computer Vision*, 2nd ed., 2004.
- [29] D. Nistér, “An efficient solution to the five-point relative pose problem,” *TPAMI*, 2004.
- [30] R. Hartley, “In defense of the eight-point algorithm,” *TPAMI*, 1997.
- [31] G. H. Lee, B. Li, M. Pollefeys, and F. Fraundorfer, “Minimal solutions for pose estimation of a multi-camera system,” *IJRR*, 2013.
- [32] D. W. Eggert, A. Lorusso, and R. B. Fisher, “Estimating 3-d rigid body transformations: a comparison of four major algorithms,” *Machine Vision and Applications*, 1997.
- [33] P. J. Besl and N. D. McKay, “A method for registration of 3-d shapes,” *TPAMI*, 1992.
- [34] R. Ranftl, K. Lasinger, D. Hafner, K. Schindler, and V. Koltun, “Towards robust monocular depth estimation: Mixing datasets for zero-shot cross-dataset transfer,” *TPAMI*, 2020.
- [35] R. Ranftl, A. Bochkovskiy, and V. Koltun, “Vision transformers for dense prediction,” *ICCV*, 2021.

- [36] L. Yang, B. Kang, Z. Huang, X. Xu, J. Feng, and H. Zhao, "Depth anything: Unleashing the power of large-scale unlabeled data," *CVPR*, 2024.
- [37] S. Wang, V. Leroy, Y. Cabon, B. Chidlovskii, and J. Revaud, "Dust3r: Geometric 3d vision made easy," *CVPR*, 2024.
- [38] V. Balntas, S. Li, and V. A. Prisacariu, "Relocnet: Continuous metric learning relocalisation using neural nets," *ECCV*, 2018.
- [39] D. Winkelbauer, M. Denninger, and R. Triebel, "Learning to localize in new environments from synthetic training data," *ICRA*, 2021.
- [40] K. Chen, N. Snavely, and A. Makadia, "Wide-baseline relative camera pose estimation with directional learning," *CVPR*, 2021.
- [41] S. En, A. Lechervy, and F. Jurie, "Rpnet: an end-to-end network for relative camera pose estimation," *ECCV*, 2018.
- [42] M. A. Fischler and R. C. Bolles, "Random sample consensus: a paradigm for model fitting with applications to image analysis and automated cartography," *CACM*, 1981.
- [43] E. Brachmann, A. Krull, S. Nowozin, J. Shotton, F. Michel, S. Gumhold, and C. Rother, "Dsac — differentiable ransac for camera localization," *CVPR*, 2016.
- [44] E. Brachmann and C. Rother, "Neural- Guided RANSAC: Learning where to sample model hypotheses," in *ICCV*, 2019.
- [45] A. Barroso-Laguna, S. Munukutla, V. Prisacariu, and E. Brachmann, "Matching 2d images in 3d: Metric relative pose from metric correspondences," *CVPR*, 2024.
- [46] B. Roessle and M. Nießner, "End2end multi-view feature matching with differentiable pose optimization," *ICCV*, 2023.
- [47] A. Kolesnikov, A. Dosovitskiy, D. Weissenborn, G. Heigold, J. Uszkoreit, L. Beyer, M. Minderer, M. Dehghani, N. Houlsby, S. Gelly, T. Unterthiner, and X. Zhai, "An image is worth 16x16 words: Transformers for image recognition at scale," *ICLR*, 2021.
- [48] V. Leroy, Y. Cabon, and J. Revaud, "Grounding image matching in 3d with mast3r," *ArXiv*, 2024.
- [49] M. Humenberger, Y. Cabon, N. Guérin, J. Morat, J. Revaud, P. Rerole, N. Pion, C. R. de Souza, V. Leroy, and G. Csurka, "Robust image retrieval-based visual localization using kapture," *ArXiv*, 2020.
- [50] O. Chum, J. Matas, and J. Kittler, "Locally optimized ransac," *Joint Pattern Recognition Symposium*, 2003.
- [51] G. Grisetti, T. Guadagnino, I. Aloise, M. Colosi, B. Della Corte, and D. Schlegel, "Least squares optimization: From theory to practice," *Robotics*, 2020.
- [52] J. Lee, *Introduction to Smooth Manifolds*, ser. Graduate Texts in Mathematics. Springer, 2003.
- [53] J. Solà, J. Deray, and D. Atchuthan, "A micro lie theory for state estimation in robotics," *ArXiv*, 2018.
- [54] K. MacTavish and T. D. Barfoot, "At all costs: A comparison of robust cost functions for camera correspondence outliers," *Conference on Computer and Robot Vision*, 2015.
- [55] A. E. Beaton and J. W. Tukey, "The fitting of power series, meaning polynomials, illustrated on band-spectroscopic data," *Technometrics*, 1974.
- [56] P. J. Huber, "Robust estimation of a location parameter," *Annals of Mathematical Statistics*, 1964.
- [57] Y. Zhou, C. Barnes, J. Lu, J. Yang, and H. Li, "On the continuity of rotation representations in neural networks," *CVPR*, 2018.